

Robot Skin with Touch and Bend Sensing using Electrical Impedance Tomography

Haofeng Chen¹, Bin Li², Bedrich Himmel¹, Xiaojie Wang², Matej Hoffmann¹

Abstract—Flexible electronic skins that simultaneously sense touch and bend are desired in several application areas, such as to cover articulated robot structures. This paper introduces a flexible tactile sensor based on Electrical Impedance Tomography (EIT), capable of simultaneously detecting and measuring contact forces and flexion of the sensor. The sensor integrates a magnetic hydrogel composite and utilizes EIT to reconstruct internal conductivity distributions. Real-time estimation is achieved through the one-step Gauss-Newton method, which dynamically updates reference voltages to accommodate sensor deformation. A convolutional neural network is employed to classify interactions, distinguishing between touch, bending, and idle states using pre-reconstructed images. Experimental results demonstrate an average touch localization error of 5.4 mm (SD 2.2 mm) and average bending angle estimation errors of 1.9° (SD 1.6°). The proposed adaptive reference method effectively distinguishes between single- and multi-touch scenarios while compensating for deformation effects. This makes the sensor a promising solution for multimodal sensing in robotics and human-robot collaboration.

I. INTRODUCTION

The importance of endowing robots with touch has been recognized for several decades and a large number of technologies have been developed (e.g., [1], [2] for surveys). The focus has largely been on tactile sensing for manipulation, as equipping robot fingers or hands with tactile sensors requires only relatively small patches of electronic skin. Whole-body artificial skins for robots have been an exception, with only few successful solutions such as [3], [4]. The potential of sensing over the whole body surface has also not been fully explored. Cheng et al. provide an overview of applications of their electronic skin in [5].

Even for the so-called whole-body skins [5], [6], it is not the complete surface of the robot that is covered. In particular the areas around the robot joints are typically without skin coverage. Complete coverage would be desired for both physical and social Human-Robot Interaction [7], [8]. The main challenge for articulated robots lies in sustaining large deformation and stretch while still delivering touch information. While measuring the angle of deformation (bending) may not be key for classical robots, which have accurate joint encoders, bending information may be relevant

¹Haofeng Chen, Bedrich Himmel, Matej Hoffmann are with the Department of Cybernetics, Faculty of Electrical Engineering, Czech Technical University in Prague.

²Bin Li and Xiaojie Wang are with the Institute of Intelligent Machines, Hefei Institutes of Physical Science, Chinese Academy of Sciences, Hefei 230031, China.

This work was co-funded by the European Union under the project Robotics and Advanced Industrial Production (reg. no. CZ.02.01.01/00/22_008/0004590).

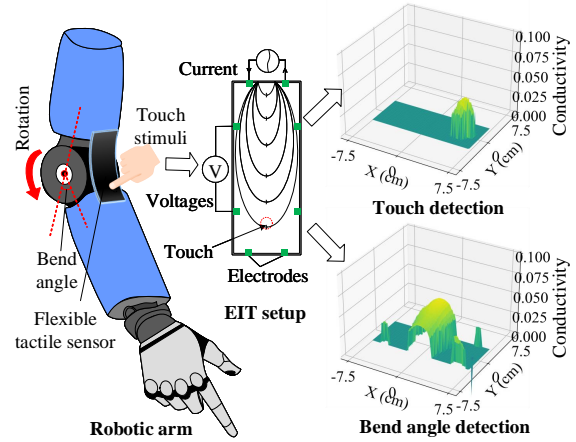


Fig. 1. Overview of EIT-based flexible tactile sensor for simultaneous touch and bending sensing.

in soft robots, providing valuable information about their body configuration (see e.g., [9]).

While soft and flexible tactile sensors have been explored, existing solutions often lack the ability to simultaneously detect and sense touch and bending. For example, Kramer et al. [10] developed a soft curvature sensor for joint angle tracking, but it cannot sense touch. Noda et al. [11] introduced a stretchable liquid-based tactile sensor with a dual-channel design, but its low spatial resolution limits multi-touch sensing. Totaro et al. [12] proposed a multimodal mechanosensing system using resistive and optical components, capable of distinguishing between pressure and bending. However, it only supports single-point touch sensing. Zhang et al. [13] designed a high-sensitivity microwave-based sensor capable of sensing both pressure and bending, but its reliance on electromagnetic coupling restricts it to small, localized areas. These limitations highlight the need for a solution that integrates touch and deformation measurements with high spatial resolution and scalability.

Electrical Impedance Tomography (EIT) presents a promising alternative for distributed sensing without requiring multiple discrete sensor units, making it well suited for whole-body robotic applications. Prior research has explored EIT for touch sensing, such as Kato et al. [14], who developed a soft, pressure-sensitive EIT-based tactile sensor for finger touch sensing. Similarly, and Park et al. [15], who introduced a large-area, face-shaped EIT sensor for multi-touch recognition. EIT has also been applied to shape sensing in soft robots, with Avery et al. [16] and Xin et al. [17]

using it to map deformations in real time. However, these approaches either lack touch sensing or require complex hardware, limiting their practicality for real-time applications. Dong et al. [18] demonstrated 3D-scanner-assisted EIT for tactile interaction mapping on deformable surfaces, but their approach required complex hardware and was not suitable for real-time applications. Despite these advancements, few studies have addressed simultaneous sensing of touch and bending in large-deformation robotic applications using EIT.

The primary challenge in achieving simultaneous touch and bending sensing using EIT lies in signal coupling—both touch and bending alter the impedance distribution in a complex manner, making it difficult to separate their effects. Additionally, EIT is an ill-posed inverse problem, where small measurement variations can lead to significant reconstruction errors, especially under large deformations.

In this paper, we present a dual-modal EIT-based flexible tactile sensor, capable of simultaneously sensing both external touch and bending of the sensor. As shown in Fig. 1, the sensor integrates EIT into the robotic arm, enabling it to track bending angles and localize touch positions through conductivity distribution analysis. EIT reconstructs internal conductivity patterns by applying electrical currents and measuring boundary voltages via surface electrodes. Touch interactions generate localized conductivity peaks, whereas bending induces distributed conductivity variations. To address signal coupling, our system employs a dynamic reference framework: (1) a pre-reconstruction step estimates initial conductivity distribution, (2) a classification step distinguishes between touch and bending, (3) bending-induced variations update the reference dynamically, and (4) touch sensing is refined using the updated reference, ensuring precise localization.

II. METHODS AND SYSTEM DESIGN

A. Working Principle of EIT for Multimodal Sensing

The EIT reconstruction problem maps the internal conductivity distribution of a conductive domain using known excitation currents and measured boundary voltages. This study employs time-difference EIT, a technique focused on visualizing conductivity variations between two observed states [19]. In difference imaging, the connection between the change in conductivity, $\Delta\sigma \in \mathbb{R}^N$, and the change in measured voltage, $\Delta\mathbf{V} \in \mathbb{R}^M$, can be approximated as a linear relationship:

$$\Delta\mathbf{V} = \mathbf{J}\Delta\sigma + \mathbf{n}_{noise} \quad (1)$$

where the sensitivity matrix $\mathbf{J} \in \mathbb{R}^{M \times N}$ ($M \ll N$), also known as the Jacobian matrix, is computed using the finite element method (FEM). Each element of \mathbf{J} is given by $J_{mn} = \left. \frac{\partial \Delta v_m}{\partial \Delta \sigma_n} \right|_{\sigma_0}$, representing the sensitivity of voltage changes to conductivity variations. Additionally, $\mathbf{n}_{noise} \in \mathbb{R}^M$ accounts for measurement noise. We define the conductivity change vector as $\Delta\sigma = [\Delta\sigma_1, \Delta\sigma_2, \dots, \Delta\sigma_N]$, where $\Delta\sigma_i = \sigma_i - \sigma_0$. Here, σ_0 is the background conductivity, and

σ_i is the conductivity of the i -th element. Similarly, the voltage change vector $\Delta\mathbf{V} = [\Delta v_1, \Delta v_2, \dots, \Delta v_M]$ is calculated as $\Delta v_i = v_i - v_i^{ref}$, where $\mathbf{V}^{ref} = [v_1^{ref}, v_2^{ref}, \dots, v_M^{ref}]$ is the reference voltage vector and $\mathbf{V} = [v_1, v_2, \dots, v_M]$ is the current voltage vector.

In this work, the one-step Gauss-Newton method is employed to solve the EIT inverse problem due to its ability to deliver fast, real-time estimation. By leveraging time-difference imaging [20], the relationship between the reconstructed conductivity changes $\Delta\sigma$ and the measured boundary voltage variations $\Delta\mathbf{V}$ can be expressed as follows:

$$\Delta\sigma = (\mathbf{J}^T \mathbf{J} + \lambda^2 \mathbf{R})^{-1} \mathbf{J}^T \Delta\mathbf{V} \quad (2)$$

where, \mathbf{J}^T represents the transpose of the Jacobian matrix \mathbf{J} , λ is a scalar hyperparameter, which is set to 0.2 to balance image resolution and noise suppression. \mathbf{R} denotes the regularization matrix. The matrix \mathbf{R} is computed using the Newton's One-Step Error Reconstructor (NOSER) prior [21].

Traditionally, EIT tactile sensors were installed on fixed surfaces with minimal bending or deformation, allowing the reference voltage \mathbf{V}^{ref} to remain constant. However, in this study, the sensor must accurately sense touch even when bent, necessitating dynamic updates to the reference voltage for differential imaging.

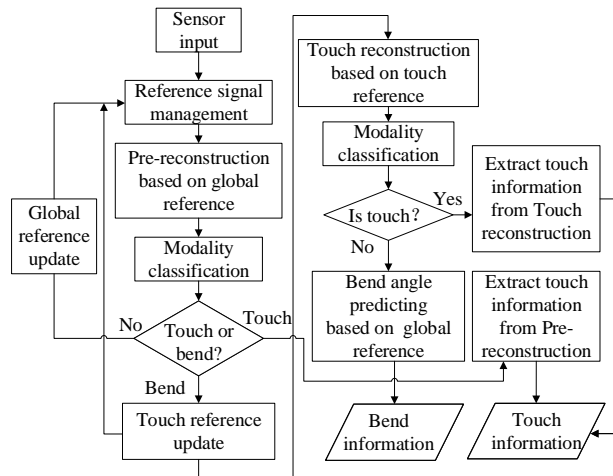


Fig. 2. Flowchart of touch and bend sensing with adaptive reference.

Figure 2 illustrates the flowchart of the proposed method, which dynamically updates the reference voltage to enable simultaneous touch and bending detection and measurement. The process begins with sensor input signals being processed through a reference signal management module, which establishes stable signal baselines. A global voltage reference—collected when the sensor is undeformed—is used for pre-reconstruction, generating an initial estimate of the sensor's state. Modality classification then determines whether the input corresponds to touch or bending.

If bending is detected, the touch reference (collected after bending) is updated to account for dynamic changes, ensuring accurate touch sensing. For touch sensing, a dedicated

reconstruction process is executed based on the updated touch reference, followed by modality classification to confirm touch presence. If touch is identified, detailed touch information is extracted; if bending is detected, the system predicts the bending angle using the global reference while refining touch-related data from the pre-reconstruction step.

This framework integrates global and dynamic touch references, enabling robust classification and extraction of touch and bending information. By employing a dual reconstruction approach, the system adapts to varying conditions, ensuring high accuracy in simultaneous touch and bending measurements.

B. Touch and bending classification

The proposed network classifies bending and touch actions using a three-module architecture, as shown in Figure 3. It takes 96×96 pre-reconstructed images generated by the one-step Gauss-Newton algorithm as input. A preprocessing module first applies threshold segmentation (threshold = 0.5) to enhance robustness and feature distinction. The core feature extraction module follows an encoder-decoder structure, where the encoder progressively extracts hierarchical features through convolutional layers ($16 \rightarrow 32 \rightarrow 64$) with 3×3 filters, batch normalization, and ReLU activation. Max pooling (2×2 , stride 2) reduces spatial dimensions while preserving key information. The decoder mirrors this process, using upsampling (2×2) and transposed convolutions ($32 \rightarrow 16$) to reconstruct spatial features, culminating in a final transposed convolution layer. The classification module then processes the extracted features through dense layers ($256 \rightarrow 128 \rightarrow 16$) with dropout regularization (rate = 0.1), producing a three-class softmax output.

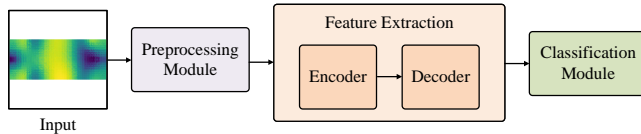


Fig. 3. Overview of the proposed bend and/or touch classification network architecture.

C. Magnetic Hydrogel-based Tactile sensor fabrication

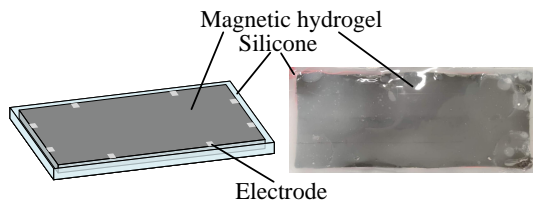


Fig. 4. Illustration of an 8-Electrode EIT Tactile Sensor. (Left) Schematic of the magnetic hydrogel-based EIT tactile sensor. (Right) Photograph of the sensor.

The selection of a magnetic hydrogel composite as the sensing layer in this study is primarily driven by its enhanced mechanical stability and exceptional pressure-sensing capabilities when combined with EIT [22]. To

achieve these properties, the magnetic hydrogels were synthesized through monomer polymerization and crosslinking, using acrylamide (AAM) as the monomer, N,N' -methylenebisacrylamide (MBAA) as the crosslinker, ammonium persulfate (APS) as the initiator, and tetramethylethylenediamine (TEMED) as the accelerator. Magnetic particles (CIPs) were incorporated at a volume fraction of 3%. First, AAM was dissolved in deionized water under continuous stirring to form a uniform solution. The initiator APS and crosslinker MBAA were then added, followed by vigorous stirring for 5 minutes to ensure homogeneity. TEMED was introduced last, and the mixture was stirred for an additional 3 minutes until fully dissolved. The resulting solution was injected into a mold, sealed, and left at room temperature to undergo gelation, yielding the magnetic hydrogel composite.

As shown in Fig. 4, the tactile sensor is composed of three primary components: a silicone layer, a magnetic hydrogel sensing layer, and eight silver electrodes uniformly distributed along the boundaries. The sensor has overall dimensions of $160 \text{ mm} \times 70 \text{ mm} \times 12 \text{ mm}$, while the magnetic hydrogel layer measures $150 \text{ mm} \times 60 \text{ mm} \times 5 \text{ mm}$. Each of the 8 silver electrodes interfaces with the conductive layer through a contact area of $5 \text{ mm} \times 5 \text{ mm}$. To prevent moisture loss, the sensing material is encapsulated using Ecoflex 30 silicone rubber, which helps maintain the hydration state of the hydrogel and ensures the long-term stability of its performance. Components A and B of the silicone were mixed at a 1:1 weight ratio, stirred thoroughly, and degassed to eliminate air bubbles. The mixture was then cast into a mold, fully encapsulating the magnetic hydrogel. After curing at room temperature for 2–3 hours, a protective silicone layer was formed, ensuring the hydrogel's stability and functionality.

D. Sensing system

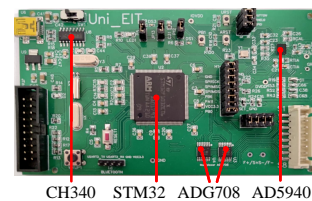


Fig. 5. The EIT circuit board.

A 16-electrode data acquisition circuit was designed (Figure 5). An AD5940 impedance measurement IC is used, capable of 0–200 kHz signal generation and 200 kHz bandwidth measurements [23]. A 40 kHz excitation balances speed and accuracy, consistent with existing EIT systems [24], [25]. Four 16:1 multiplexers (ADG706) enable sequential electrode addressing. A 4-wire approach [23] measures impedance changes. This acquires 120 values from unique electrode pairs without repetition. A microcontroller (STM32) controls the multiplexers, coordinates the AD5940, and transfers data to a computer. Further implementation details are in [26].

III. TACTILE SENSOR EXPERIMENT

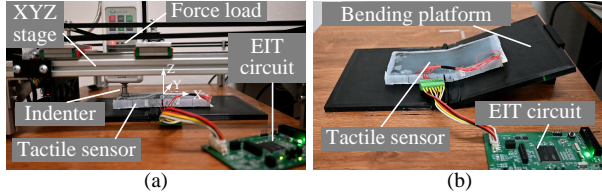


Fig. 6. Experimental setups for (a) Touch test; (b) Bending test.

Experiments were conducted to evaluate the touch sensing and bending angle estimation capabilities of the proposed EIT-based tactile sensor. As shown in Figure 6 (a), a controlled indentation test was performed using an experimental setup where the sensor was fixed horizontally, and a 15 mm diameter indenter was mounted on a computer-controlled XYZ stage. The stage was programmed to move along the z-axis to apply indentation forces, which were precisely measured using an inline commercial force gauge (Sauter FH100). For the bending experiments, the sensor was mounted on a platform with manually adjustable angles of 0° to 60° in 10° increments, as shown in Figure 6 (b).

A. Single touch test

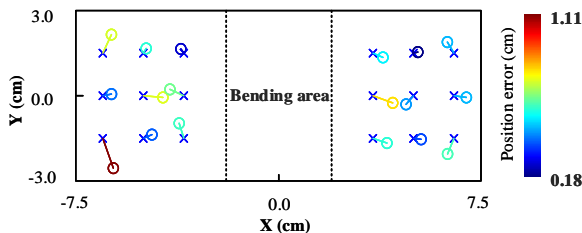


Fig. 7. Touch position error results.

The sensor's touch localization accuracy was evaluated by measuring the error between the reconstructed compressed area's centroid and the actual indenter position. A 15 mm diameter indenter applied a constant 10 N force at 18 different positions, spaced 15 mm apart along both the x- and y-axes. The touch location was determined using the method described in [26]. As shown in Figure 7, the average localization error was 5.4 ± 2.2 mm. The sensing region was divided into a touch area and a bending area (currently set to 4 cm in length). Due to its distance from the electrodes, the bending area exhibited lower touch localization accuracy. Future improvements could include adding more electrodes near this region to enhance touch sensing precision.

B. Touch or bending classification test

To classify different sensor interactions—touch, bending, and idle states—a supervised learning approach was implemented. The training dataset comprised 1,080 samples, ensuring a balanced representation of each condition. Bending data included 225 samples collected across 15 different angles ranging from 0° to 60°, while touch data consisted

of 315 samples recorded from 21 randomly selected contact locations. Additionally, 500 samples were gathered for the no-action case to account for the sensor's baseline state. The dataset was split into 80% for training and 20% for testing. A deep learning model was trained using sparse categorical cross-entropy loss, with a batch size of 64 and 100 training epochs to optimize classification performance.

The model achieved a perfect classification accuracy of 100% on the test set. While this preliminary study demonstrates the feasibility of distinguishing between these three simple actions, the classification task remains relatively straightforward due to the distinct signal patterns associated with each action. Future studies will explore more complex interactions and refine the model's capability to handle subtle variations in sensor responses.

C. Bending test

To establish a quantitative relationship between sensor voltage changes and bending angles, we adopted a data-driven approach combining feature selection and regression modeling. The experiment involved systematic measurements at six bending angles (0°, 10°, 20°, 30°, 40°, and 50°), with 15 time-series samples recorded for each to ensure statistical robustness.

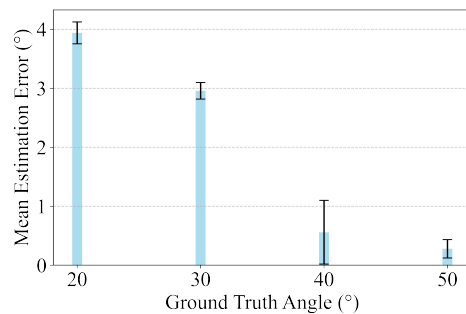


Fig. 8. Bending angle estimation error.

Given the high-dimensional nature of the voltage response data, we first applied a feature selection step by leveraging the discrete nature of the bending angles. Using the ANOVA F-test (SelectKBest) [27], we identified the five most relevant voltage features based on their correlation with bending variations, effectively reducing dimensionality and focusing on the most informative signals. These selected features were then used to train a linear regression model, establishing a direct mapping between voltage changes and bending angles.

The angle estimation performance of the system was evaluated by comparing the estimated angles to the ground truth values (20°, 30°, 40°, and 50°) using five repeated measurements for each angle. The mean estimation errors were 3.94°, 2.96°, 0.56°, and 0.28°, respectively, for the ground truth angles, as shown in Figure 8. The standard deviations were 0.19°, 0.14°, 0.54°, and 0.16°, respectively, indicating consistent performance across repeated measurements, particularly at higher angles. The overall mean absolute error across all measurements was 1.94° with a standard deviation of

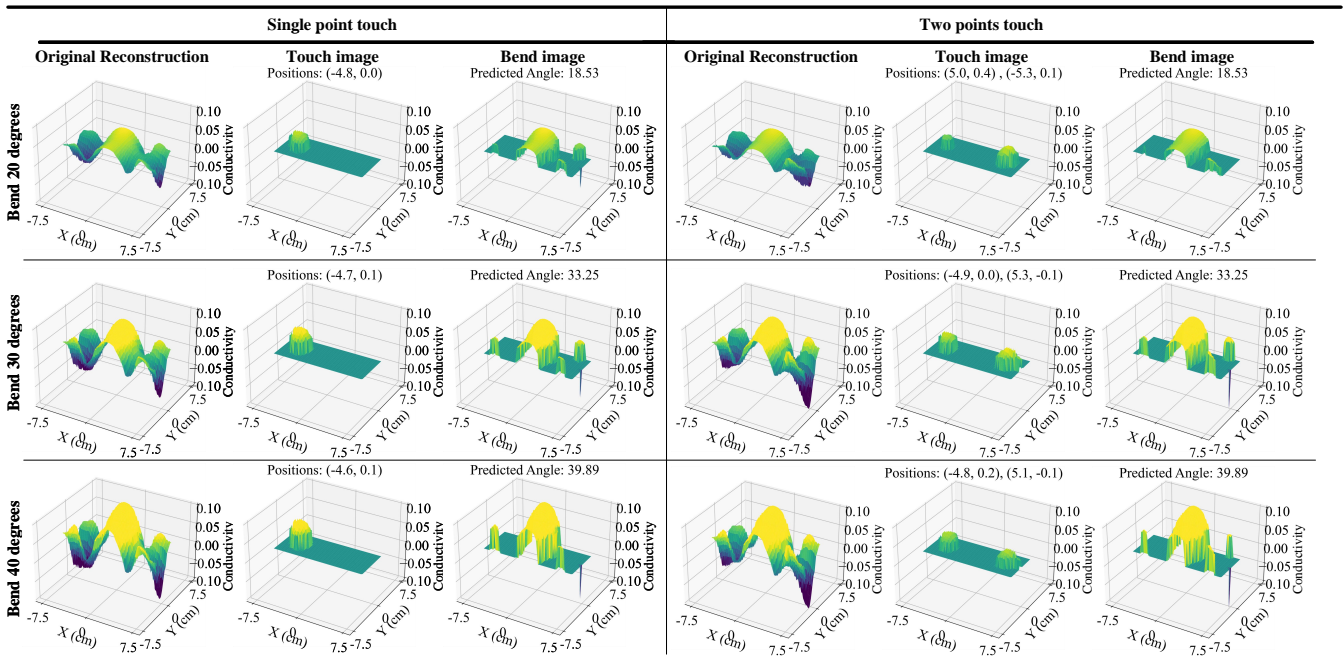


Fig. 9. Reconstructed touch positions and bending angles for single and two-point interactions using the proposed sensor.

1.73°. The results showed that the estimation error decreased significantly with increasing angle, with the smallest error observed at 50°. These findings demonstrate that the system achieves reliable angle estimation, particularly for larger bending angles. The real-time response of our system in the bending test is demonstrated in the accompanying video.

D. Simultaneous touch and bend test

The proposed tactile sensor effectively integrates touch and bend sensing, as illustrated in Figure 9. This figure presents representative real-time examples of single-point and two-point touch tests conducted at three different bending angles using the proposed adaptive reference method (see also video).

Taking single-point touch as an example, the first column shows the original reconstruction obtained using a one-step Gauss-Newton method with a global reference collected when the sensor was undeformed. The second column presents the reconstructed touch image based on an adaptive touch reference, which is collected after bending. The third column shows the reconstructed bending image, also based on a global reference, but with a thresholding method applied to filter out regions with conductivity values below zero. This enhances the visibility of conductivity changes in the curved area.

The original reconstruction image couples both touch and bending information when bending and touch occur simultaneously, making it challenging to isolate the touch response under bending conditions. However, applying the adaptive reference method allows for clear extraction of touch information while also enabling accurate bending angle estimation.

The sensor demonstrates reliable reconstruction of both touch positions and bending angles across various conditions, with separate evaluations for single-point and two-point touches. For single-point touch estimation, the sensor achieves a mean location error of 0.31 cm. For two-point touches, the mean errors are 0.23 cm and 0.29 cm for each tested point, respectively.

IV. APPLICATION ON A HUMANOID ROBOT

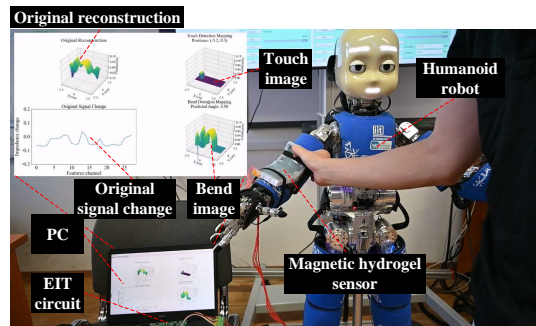


Fig. 10. Deployment and testing of the sensor on the elbow joint of a humanoid robot.

The iCub humanoid robot has large areas of its body covered with sensitive electronic skin based on capacitive technology [6], [28]. Overall, there are 4000 pressure-sensitive receptors. This large-area coverage can be effectively employed in human-robot interaction (e.g., [29]). However, the coverage of the robot surface is not complete and the joints constitute large areas not covered. To mitigate this problem and motivate the potential uses of the sensor developed in this work, we have attached the sensor patch

over the elbow joint of the iCub robot, as shown in Figure 10. The system comprises three key components: a humanoid robot arm platform, an EIT data acquisition circuit, and magnetic hydrogel-based tactile sensors installed over the elbow joint—a critical region lacking tactile sensing in the original iCub design. This integration enables simultaneous sensing of touch and bending.

The PC serves as the central hub for real-time EIT reconstruction and visualization, displaying multiple outputs: the original reconstruction, which represents the global voltage-based image; raw signal changes, which reflect boundary voltage variations, converted to impedance values for visualization; the reconstructed touch image; and the reconstructed bending image.

Figure 11 presents snapshots of the real-time physical interaction experiments using our dual-modal EIT tactile sensor (see video). In Figure 11 (a), when neither touch nor bending is applied, the raw signal changes remain near zero, the touch and bend images remain black, the touch position displays “none,” and the predicted bending angle is 0.00° . In Figure 11 (b), a small bending angle is introduced. The bend image shows an increase in reconstructed conductivity corresponding to the bending angle, which is predicted as 3.59° . The touch position remains “none,” and the touch image remains blank. In Figure 11 (c), while maintaining the small bend angle, a fingertip touch is applied. The touch image reconstructs the contact location in 3D, and the position data (4.6, 0.5) closely matches the actual touch point. In Figure 11 (d), both bending and touch are applied with a larger deflection angle. The system successfully detects and reconstructs both interactions simultaneously, demonstrating its capability to enhance the robot’s physical interaction awareness.

Despite these advancements, real-world robotic applications present challenges, such as variations in bending positions that may introduce discrepancies compared to the training data, potentially affecting estimation accuracy. To address this, future improvements could incorporate adaptive learning algorithms or real-time calibration mechanisms to enhance the system’s robustness and generalization.

V. CONCLUSION

This study presents a novel EIT-based flexible tactile sensor system designed to address the challenge of simultaneously detecting and sensing touch and bending of a soft skin patch. By implementing an adaptive reference method and advanced signal processing techniques, our sensor shows promising performance in distinguishing and measuring touch and bending interactions. Experimental results confirm the system’s effectiveness, demonstrating strong accuracy in touch localization and bending angle estimation under the tested conditions. The successful integration of the sensor into a humanoid robot arm platform highlights its practical application potential.

While the system shows great promise, it is currently limited to simple bending movements and cannot handle more complex motions, such as twisting. Future work should

focus on extending the sensor’s capabilities to accommodate these more complex deformations. Additional improvements could include increasing electrode density in the bending area, applying adaptive learning algorithms for enhanced robustness, and developing real-time calibration mechanisms for dynamic environments. We are committed to refining the EIT sensor design to better address these challenges, with the goal of creating a more versatile and robust sensing solution for advanced robotic applications, which may include also soft robots.

REFERENCES

- [1] C. Bartolozzi, L. Natale, F. Nori, and G. Metta, “Robots with a sense of touch,” *Nature materials*, vol. 15, no. 9, pp. 921–925, 2016.
- [2] R. Dahiya, D. Akinwande, and J. S. Chang, “Flexible electronic skin: From humanoids to humans [scanning the issue],” *Proceedings of the IEEE*, vol. 107, no. 10, pp. 2011–2015, 2019.
- [3] G. Cannata, M. Maggiali, G. Metta, and G. Sandini, “An embedded artificial skin for humanoid robots,” in *2008 IEEE International conference on multisensor fusion and integration for intelligent systems*. IEEE, 2008, pp. 434–438.
- [4] P. Mittendorfer and G. Cheng, “Humanoid multimodal tactile-sensing modules,” *Robotics, IEEE Transactions on*, vol. 27, no. 3, pp. 401–410, 2011.
- [5] G. Cheng, E. Dean-Leon, F. Bergner, J. R. G. Olvera, Q. Leboutet, and P. Mittendorfer, “A comprehensive realization of robot skin: Sensors, sensing, control, and applications,” *Proceedings of the IEEE*, vol. 107, no. 10, pp. 2034–2051, 2019.
- [6] P. Maiolino, M. Maggiali, G. Cannata, G. Metta, and L. Natale, “A flexible and robust large scale capacitive tactile system for robots,” *Sensors Journal, IEEE*, vol. 13, no. 10, pp. 3910–3917, 2013.
- [7] D. Silvera-Tawil, D. Rye, and M. Velonaki, “Artificial skin and tactile sensing for socially interactive robots: A review,” *Robotics and Autonomous Systems*, vol. 63, pp. 230–243, 2015.
- [8] G. Pang, G. Yang, and Z. Pang, “Review of robot skin: A potential enabler for safe collaboration, immersive teleoperation, and affective interaction of future collaborative robots,” *IEEE Transactions on Medical Robotics and Bionics*, vol. 3, no. 3, pp. 681–700, 2021.
- [9] T. G. Thuruthel, B. Shih, C. Laschi, and M. T. Tolley, “Soft robot perception using embedded soft sensors and recurrent neural networks,” *Science Robotics*, vol. 4, no. 26, p. eaav1488, 2019.
- [10] R. K. Kramer, C. Majidi, R. Sahai, and R. J. Wood, “Soft curvature sensors for joint angle proprioception,” in *2011 IEEE/RSJ International Conference on Intelligent Robots and Systems*. IEEE, 2011, pp. 1919–1926.
- [11] K. Noda, E. Iwase, K. Matsumoto, and I. Shimoyama, “Stretchable liquid tactile sensor for robot-joints,” in *2010 IEEE International Conference on Robotics and Automation*. IEEE, 2010, pp. 4212–4217.
- [12] M. Totaro, A. Mondini, A. Bellacicca, P. Milani, and L. Beccai, “Integrated simultaneous detection of tactile and bending cues for soft robotics,” *Soft robotics*, vol. 4, no. 4, pp. 400–410, 2017.
- [13] H. Liu, C. Yang, J. Ma, and M. Xu, “Multimodal soft sensor integrated with hydrogel-optoelectronic for wrist motion monitoring,” *Measurement*, vol. 239, p. 115486, 2025.
- [14] Y. Kato, T. Mukai, T. Hayakawa, and T. Shibata, “Tactile sensor without wire and sensing element in the tactile region based on eit method,” *SENSORS, 2007 IEEE*, pp. 792–795, 2007.
- [15] H. Park, W. Kim, S. Jeon, Y. Na, and J. Kim, “Graph-structured super-resolution for geometry-generalized tomographic tactile sensing: Application to humanoid faces,” *IEEE Transactions on Robotics*, vol. 41, pp. 558 – 572, 2024. [Online]. Available: <https://ieeexplore.ieee.org/abstract/document/10770598>
- [16] J. Avery, M. Runciman, A. Darzi, and G. P. Mylonas, “Shape sensing of variable stiffness soft robots using electrical impedance tomography,” in *2019 International Conference on Robotics and Automation (ICRA)*. IEEE, 2019, pp. 9066–9072.
- [17] W. Xin, F. Zhu, P. Wang, Z. Xie, Z. Tang, and C. Laschi, “Electrical impedance tomographic shape sensing for soft robots,” *IEEE Robotics and Automation Letters*, vol. 8, no. 3, pp. 1555 – 1562, 2023.

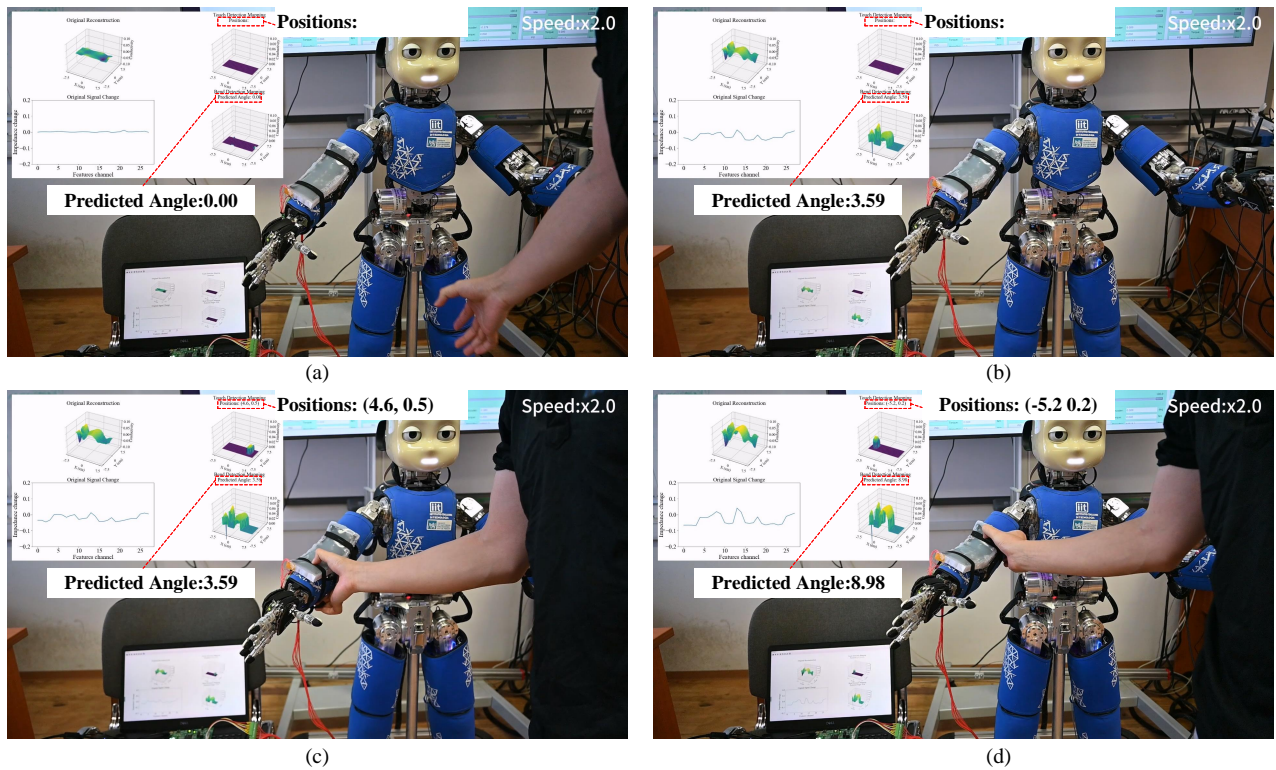


Fig. 11. Illustration of sensor operation when mounted on a humanoid robot. (a) No touch or bending is applied. (b) Slight bending, no touch interaction. (c) A fingertip touch is applied while maintaining a small bending angle. (d) Both bending and touch are applied, with a bigger bending angle.

- [18] H. Dong, Z. Liu, D. Hu, X. Wu, F. Giorgio-Serchi, and Y. Yang, "Tactile sensing on deformed surfaces with electrical impedance tomography," in *2024 IEEE International Instrumentation and Measurement Technology Conference (I2MTC)*. IEEE, 2024, pp. 1–6.
- [19] D. Silvera-Tawil, D. Rye, M. Soleimani, and M. Velonaki, "Electrical impedance tomography for artificial sensitive robotic skin: a review," *IEEE Sensors Journal*, vol. 15, no. 4, pp. 2001–2016, 2015.
- [20] A. Adler, T. Dai, and W. R. Lionheart, "Temporal image reconstruction in electrical impedance tomography," *Physiological measurement*, vol. 28, no. 7, p. S1, 2007.
- [21] M. Cheney, D. Isaacson, J. C. Newell, S. Simske, and J. Goble, "Noser: An algorithm for solving the inverse conductivity problem," *International Journal of Imaging systems and technology*, vol. 2, no. 2, pp. 66–75, 1990, linear.
- [22] B. Li, X. Yang, H. Chen, C. Xu, and X. Wang, "Flexible tactile sensing of magnetic hydrogel composites based on electrical impedance tomography," *Journal of Intelligent Material Systems and Structures*, p. 1045389X241280631, 2024.
- [23] Analog Devices, *High Precision, Impedance, and Electrochemical Front End AD5940/5941 (Data Sheet)*, Analog Devices, Norwood, MA, USA, 2020. [Online]. Available: <https://www.analog.com/media/en/technical-documentation/data-sheets/AD5940-5941.pdf>
- [24] G. Ma, Z. Hao, X. Wu, and X. Wang, "An optimal electrical impedance tomography drive pattern for human-computer interaction applications," *IEEE Transactions on Biomedical Circuits and Systems*, vol. 14, no. 3, pp. 402–411, 2020.
- [25] Y. Zhang, R. Xiao, and C. Harrison, "Advancing hand gesture recognition with high resolution electrical impedance tomography," in *Proceedings of the 29th Annual Symposium on User Interface Software and Technology*. ACM, 2016, pp. 843–850.
- [26] H. Chen, X. Yang, P. Wang, J. Geng, G. Ma, and X. Wang, "A large-area flexible tactile sensor for multi-touch and force detection using electrical impedance tomography," *IEEE Sensors Journal*, vol. 22, no. 7, pp. 7119–7129, 2022.
- [27] A. Zollanvari, *Feature Selection*. Cham: Springer International Publishing, 2023, pp. 283–302. [Online]. Available: https://doi.org/10.1007/978-3-031-33342-2_10
- [28] G. Metta, L. Natale, F. Nori, G. Sandini, D. Vernon, L. Fadiga, C. Von Hofsten, K. Rosander, M. Lopes, and J. Santos-Victor, "The iCub humanoid robot: An open-systems platform for research in cognitive development," *Neural networks*, vol. 23, no. 8-9, pp. 1125–1134, 2010.
- [29] J. Rozlivek, A. Roncone, U. Pattacini, and M. Hoffmann, "Harmonious—human-like reactive motion control and multimodal perception for humanoid robots," *IEEE Transactions on Robotics*, vol. 41, pp. 378–393, 2025.